Nonlinear Vibration Behavior of Aero-Engine Rotor-Bearing System in Maneuvering Flight

Wujiu Pan[a, b,]*, Haoyong Qu[a, b], Lele Sun[c], and Xianmu Li[a, b]

[a] *School of Mechatronics Engineering, Shenyang Aerospace University, Shenyang, 110136 PR China*

[b] *Advanced Manufacturing Technology Research Center, Shenyang Aerospace University, Shenyang, 110136 PR China*

[c] *School of Mechanical Science and Engineering, Huazhong University of Science and Technology, Wuhan, 430074 PR China*

* e-mail: panspace@sina.cn

Abstract—Analyzing the dynamic characteristics of an aero-engine rotor-bearing system helps professionals predict and judge the dynamic behavior of aero-engines. It is different from the traditional dynamic analysis of rotor system with fixed foundation, this paper considers the dynamics of the rotor-bearing system caused by the horizontal yawing maneuver load. This paper establishes a finite element model of a double-disc rotor-bearing system, and use the Newmark-β algorithm to solve the system. The model established in this paper is compared with the model established in ANSYS software, and the correctness of this model is verified. The influence of the maneuver load on the nonlinear dynamics of the rotor-bearing system under horizontal yawing is analyzed in detail. The study found, the maneuver load can suppress nonlinear vibration; the increase of maneuver load can reduce the nonlinear influence of the system caused by changes in relevant bearing parameters; and between two times the critical speed and three times the critical speed, the system will produce rich and complex nonlinear dynamic phenomena such as single periodic motion, multi periodic motion, and quasi-periodic motion.

Keywords: horizontal yawing, nonlinear analysis, double-disc rotor system, dynamic modeling

DOI: 10.3103/S0025654422601501

1. INTRODUCTION

Maneuver flight refers to the flight process in which the aircraft constantly changes its motion state (including speed, acceleration, angular velocity, angular acceleration and other flight parameters) in space, it is the unique operating environment of the aircraft rotor system, it is also an important indicator for evaluating the performance of aero-engines [1]. With the continuous development and upgrading of modern warplanes, the concept of "super maneuver flight" has been raised [2], the aircraft is required to have the ability to carry out some maneuverable tactical maneuvers after exceeding the stall angle of attack, so as to allow the aircraft to occupy a favorable position in aerial combat. When the aircraft is maneuvering, the engine rotor system will be subject to additional excitation force, namely maneuver load. The maneuver load will cause vibration instability of the system, which will threaten the safety and stability of the aero-engine [3]. Horizontal yawing is a kind of maneuver flight. Therefore, the nonlinear analysis of the rotor system [4] and the study of the dynamic behavior of aero-engine under horizontal yaw additional maneuvering load can provide a theoretical basis for the optimal design of aero-engine rotor bearing system and maneuvering load control.

Many studies on the dynamic characteristics of a rotor-bearing system have assumed that the rotor support is on a stationary basis, whether it is elastic support or rigid support [5]. Many scholars have studied the rotor system with fixed foundation. Banakh and Nikiforov [6] studied the dynamic characteristics of high-speed rotor system with floating seal ring, and obtained the motion analysis law of rotor and seal ring through curve fitting method. In order to study the motion types of nonlinear Jeffcott rotor system in a specific parameter range, Xu et al. [7] obtained the bifurcation tree of periodic 1 to periodic 8 motion in nonlinear Jeffcott rotor system by discrete mapping method, and discussed the bifurcation and stability of

periodic motion on the bifurcation tree. Ma et al. [8, 9] established the differential equations of motion and dynamics models of the internal and external dual rotor system, it shows that the unbalance of the rotor system is the main factor causing the vibration of the aero-engine. In order to analyze the lateral vibration of rotor system caused by rotating stall, Fan et al. [10, 11] used Mansoux model to couple unbalanced friction load, established the dynamic model of rotor system with transverse load caused by pressure and flow coefficient fluctuation, and studied the vibration characteristics of rotor system with and without transverse load by numerical calculation technology. In order to study the bifurcation, stability and chaotic path of nonlinear flexible rotor bearing system, Phadatare and Pratiher [12] established a large deflection model and discussed the nonlinear dynamic analysis of rotor-disc-bearing system with geometric eccentricity and mass imbalance. Cao et al. [13, 14] put forward a new dynamic modeling method of rolling bearing-rotor system based on rigid element (RBE) and analyzed the nonlinear behavior of rotor bearing system. In order to diagnose the crack in the uncertain environment, Fu et al. [15] used the combination of finite element method (FEM) and harmonic balance method (HBM), focusing on the vibration behavior of the spindle rotor system in the presence of crack under the inherent model uncertainty. In order to analyze the stability of a rigid rotor supported by ball bearings, Harsha et al. [16, 17] established a rotor rolling bearing system considering bearing clearance and waviness, and used a numerical method to analyze the non-linear dynamic effects of different parameters on the rotor-bearing system.

However, with the increasing requirements for maneuverability, flexibility and stability of military fighters in flight, it is necessary to study the dynamic behavior of aero-engine rotor system under maneuver load. In other words, in this case, the foundation of the rotor-bearing system is moving. In this regard, many scholars have also made a lot of contributions. Xu et al. [18, 19] established the transient vibration model of Jeffcott rotor system during maneuver flight, and discussed the dynamic characteristics of the rotor system during maneuver flight. Lin and Meng [20] used a Jeffcott rotor model, and studied the influence of aircraft maneuvering at constant angular velocity or constant acceleration in vertical or horizontal plane on the dynamic characteristics of aero-engine rotor system, and analyzed the influence of different flight conditions on the rotor system. In order to study the vibration characteristics of aero-engine rotor system during maneuver flight, Zhu and Chen [21] established the general motion equation of flexible rotor system under maneuver flight conditions by using Lagrange equation, the influence of aircraft maneuvering on the dynamic characteristics of rotor system was studied by numerical method. Hou et al. [22−24] established the dynamic differential equations of rotor-bearing systems with different types of supports (fixed support, cubic nonlinear elastic support and rolling bearing support) under maneuver flight conditions, and consider the faults such as rubbing and cracking, researched the effects of maneuver load on the nonlinear dynamics of the system by numerical method. In order to study the dynamic characteristics of rotor system under large maneuver conditions, Zhang et al. [25] deduced the finite element modeling method of rotor system, studied the response law of linear rotor system and nonlinear rotor system with bearing under large maneuver conditions. Gao et al. [26] established a flexible asymmetric rotor system model considering the nonlinear support of ball bearing and squeeze film damper, and systematically studied the dynamic characteristics of the rotor system under maneuver flight.

From the above research, it can be seen that many scholars do not consider the base movable condition in the research of rotor system. However, if the maneuver condition is considered, the real rotor system should move with the aircraft. At the same time, it can be seen from the third paragraph of the review that although many scholars have used different methods to study the dynamic characteristics of the rotor system under the condition of base motion, the rotor system model is a simple single-disc rotor system, and many strong nonlinear factors are not considered. In addition, the complex dynamics of an aero-engine cannot be described by a single disc rotor model. Therefore, it is necessary to establish a general analysis model considering multiple nonlinear factors. The main contributions of this paper are as follows: (1) a general aero-engine rotor-bearing-disc system model is established, which takes into account horizontal yawing maneuver load, nonlinear contact force of rolling bearing, eccentric unbalance force of disc, gravity field and gyro effect; (2) the responses of the system under maneuver loads are analyzed in detail; (3) the nonlinear response law of different bearing parameters with or without maneuver load is analyzed in detail.

This paper is mainly composed of four parts. In the Section 2, the rolling bearing model and the finite element model of the rotor-bearing system under horizontal yawing are established, which provide a theoretical basis for the dynamic analysis of the whole paper. In the Section 3, the Campbell diagram and mode shapes are compared and verified by using ANSYS finite element method, which fully proves the correctness and effectiveness of the modeling method in this paper. In the Section 4, the nonlinear dynamic behavior of the dual-disc rotor-bearing system under horizontal yawing maneuver load is studied, the influence of the maneuver load on rotor system is discussed. Section 5 presents the conclusions.
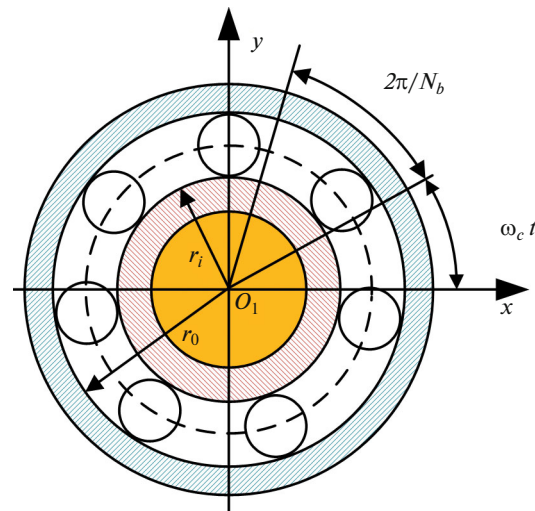
Fig. 1. Rolling bearing model.

2. FINITE ELEMENT MODELING AND SOLUTION OF THE SYSTEM UNDER HORIZONTAL YAWING

2.1. Rolling Bearing Modeling

Figure 1 is a schematic diagram of the rolling bearing model. The rolling bearing consists of inner ring, outer ring, cage and rolling element. Set the balls evenly arranged between the inner and outer raceways, there is pure rolling between the ball and the raceway. Suppose the linear velocity of the contact point between the ball and the bearing outer ring is v_o, the linear velocity of the contact point with the inner ring of the bearing is v_i, the rotation speed of the outer ring of the bearing is ω_o, the rotational angular velocity of the inner ring is ω_i, the radius of the outer raceway is R_o, the radius of the inner raceway is R_i, then $v_o = \omega_o R_o$, $v_i = \omega_i R_i$.

The linear velocity of the roller center is $v_c = (v_o + v_i)/2$. Because the fixed bearing outer ring does not rotate with the rotor, then $v_o = 0$, that is $v_c = v_i/2$, so the rotation speed of the cage is $\omega_c = (\omega_i R_i)/R_o + R_i$. The inner ring is fixed on the shaft, so $\omega_i = \omega$. The number of bearing balls is N_b, suppose the angular position of the j-th ball is θ_j. Then there is

$$\theta_j = \omega_c t + \frac{2\pi}{N_b}(i-1), \quad i = 1,2,3, \ldots, N_b \tag{1}$$

Suppose the vibration displacement of the bearing inner ring center is x, y, the bearing radial clearance is δ_0, then the contact deformation between the j-th ball and raceway is $\delta_j = y\sin\theta_j + x\cos\theta_j - \delta_0$, according to the Hertz contact theory, the bearing force can be obtained as

$$\begin{bmatrix} F_{bx} \\ F_{by} \end{bmatrix} = -K_b \sum_{j=1}^{N_b} \delta_j^{1.5} H_f(\delta_j) \begin{bmatrix} \cos\theta_j \\ \sin\theta_j \end{bmatrix}, \tag{2}$$

where K_b is the Hertz contact stiffness, H_f is the Heaviside function. The value of H_f is

$$H_f(\delta_j) = \begin{cases} 1, & \delta_j > 0, \\ 0, & \delta_j \leq 0. \end{cases} \tag{3}$$

2.2. Dynamic Differential Equation of Rotor-Rolling Bearing System under Horizontal Yawing

2.2.1. Theoretical Basis of Finite Element

In this paper, the shaft of rotor-bearing system is modeled by Rayleigh beam. There are four degrees of freedom at each node of the Rayleigh beam element. Figure 2 is the finite element model of the rotor element shaft section. Its generalized coordinate is as follows.
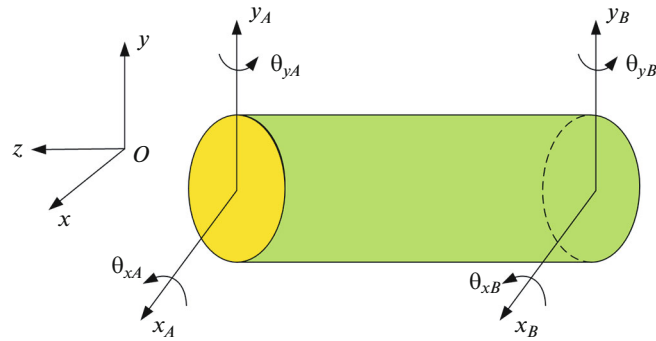
Fig. 2. The finite element model of the rotor element shaft section.

$$\mathbf{u}_s = \begin{bmatrix} x_A & y_A & \theta_{xA} & \theta_{yA} & x_B & y_B & \theta_{xB} & \theta_{yB} \end{bmatrix}^{\mathrm{T}} \tag{4}$$

The corresponding element mass matrix, element stiffness matrix and gyro force matrix of the Rayleigh beam [27] can be obtained in the form as follows.

$$\mathbf{M}_s^R = \frac{\rho\pi(r_o^4 - r_i^4)}{120l} \begin{bmatrix} 36 & 0 & 0 & 3l & -36 & 0 & 0 & 3l \\ 0 & 36 & -3l & 0 & 0 & -36 & -3l & 0 \\ 0 & -3l & 4l^2 & 0 & 0 & 3l & -l^2 & 0 \\ 3l & 0 & 0 & 4l^2 & -3l & 0 & 0 & -l^2 \\ -36 & 0 & 0 & -3l & 36 & 0 & 0 & -3l \\ 0 & -36 & 3l & 0 & 0 & 36 & 3l & 0 \\ 0 & -3l & -l^2 & 0 & 0 & 3l & 4l^2 & 0 \\ 3l & 0 & 0 & -l^2 & -3l & 0 & 0 & 4l^2 \end{bmatrix}, \tag{5}$$

$$\mathbf{M}_s^T = \frac{\rho\pi(r_o^2 - r_i^2)l}{420} \begin{bmatrix} 156 & 0 & 0 & 22l & 54 & 0 & 0 & -13l \\ 0 & 156 & -22l & 0 & 0 & 54 & 13l & 0 \\ 0 & -22l & 4l^2 & 0 & 0 & -13l & -3l^2 & 0 \\ 22l & 0 & 0 & 4l^2 & 13l & 0 & 0 & -3l^2 \\ 54 & 0 & 0 & 13l & 156 & 0 & 0 & -22l \\ 0 & 54 & -13l & 0 & 0 & 156 & 22l & 0 \\ 0 & 13l & -3l^2 & 0 & 0 & 22l & 4l^2 & 0 \\ -13l & 0 & 0 & -3l^2 & -22l & 0 & 0 & 4l^2 \end{bmatrix}, \tag{6}$$

$$\mathbf{K}_s = \frac{E\pi(r_o^4 - r_i^4)}{4l^3} \begin{bmatrix} 12 & 0 & 0 & 6l & -12 & 0 & 0 & 6l \\ 0 & 12 & -6l & 0 & 0 & -12 & -6l & 0 \\ 0 & -6l & 4l^2 & 0 & 0 & 6l & 2l^2 & 0 \\ 6l & 0 & 0 & 4l^2 & -6l & 0 & 0 & 2l^2 \\ -12 & 0 & 0 & -6l & 12 & 0 & 0 & -6l \\ 0 & -12 & 6l & 0 & 0 & 12 & 6l & 0 \\ 0 & -6l & 2l^2 & 0 & 0 & 6l & 4l^2 & 0 \\ 6l & 0 & 0 & 2l^2 & -6l & 0 & 0 & 4l^2 \end{bmatrix}, \tag{7}$$
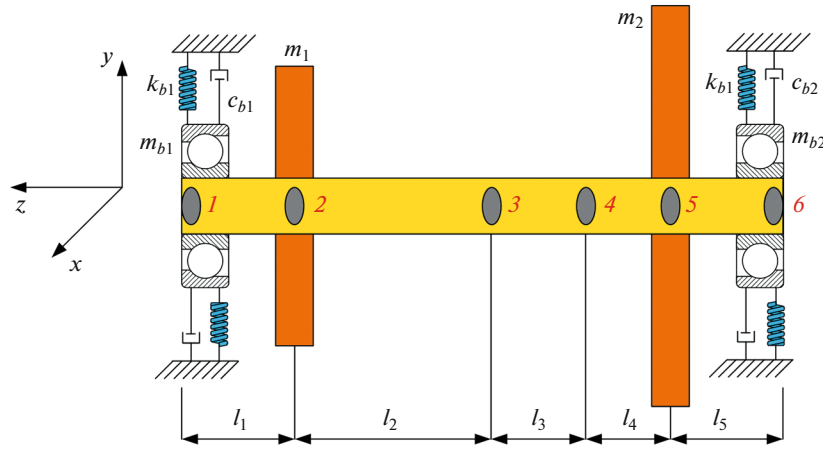
Fig. 3. Physical model of the rotor-rolling bearing system.

$$\mathbf{G}_s = \frac{\rho\pi(r_o^4 - r_i^4)}{60l} \begin{bmatrix} 0 & -36 & 3l & 0 & 0 & 36 & 3l & 0 \\ 36 & 0 & 0 & 3l & -36 & 0 & 0 & 3l \\ -3l & 0 & 0 & 4l^2 & -3l & 0 & 0 & -l^2 \\ 0 & -3l & 4l^2 & 0 & 0 & -3l & l^2 & 0 \\ 0 & 36 & -3l & 0 & 0 & 36 & 3l & 0 \\ -36 & 0 & 0 & -3l & 36 & 0 & 0 & 3l \\ -3l & 0 & 0 & l^2 & 3l & 0 & 0 & 4l^2 \\ 0 & -3l & -l^2 & 0 & 0 & 3l & 4l^2 & 0 \end{bmatrix}, \tag{8}$$

where E is the elastic modulus of the material, ρ is the density of the material, r_o and r_i are the outer radius and the inner radius of the shaft respectively, l is the length of the element shaft section.

2.2.2. Modeling the Rotor-Bearing System under Horizontal Yawing

Figure 3 shows the physical model of the rotor-rolling bearing system. An angular velocity ω_y around the y axis is the horizontal yawing flight. m_1, m_2, m_{b1}, m_{b2} are the lumped masses of disc 1, disc 2, left end bearing outer ring, and right end bearing outer ring respectively; e_1, e_2 are the eccentricity of disc 1 and disc 2 respectively; J_{pi} and J_{di} ($I = 1, 2$) are the polar moment of inertia and diameter moment of inertia of disc 1 and disc 2, respectively; k_{b1} and k_{b2} are the connection stiffness of the bearing seat and the outer ring of the left end bearing and the outer ring of the right end bearing respectively; C_{b1} and C_{b2} are the connection damping of the bearing seat and the outer ring of the left end bearing and the outer ring of the right end bearing respectively.

According to the structural characteristics of the rotor-bearing system, the rotor-bearing system is divided into 5 elements and 6 nodes. Two rolling bearings are located at node 1 and node 6.

By using the finite element method, the above finite element model group of rotor-bearing system is integrated into the following dynamic differential equations.

$$\mathbf{M}\ddot{\mathbf{X}} + (\mathbf{C} - \omega\mathbf{G} + \mathbf{C}_b)\dot{\mathbf{X}} + (\mathbf{K} + \mathbf{K}_b)\mathbf{X} = \mathbf{F}_e + \mathbf{F}_b + \mathbf{F}_h + \mathbf{G}_1, \tag{9}$$

where $\mathbf{M}$ is the mass matrix, $\mathbf{C}$ is the material damping matrix, $\mathbf{G}$ is the gyroscopic matrix, $\mathbf{K}$ is the stiffness matrix, ω is the rotor speed, $\mathbf{F}_e$ is the unbalanced force vector of centrifugal force, $\mathbf{F}_b$ is the nonlinear Hertz contact force vector of the rolling bearing, $\mathbf{C}_b$ and $\mathbf{K}_b$ are the additional damping matrix and stiffness matrix due to maneuver flight, $\mathbf{F}_h$ is the maneuver load vector, $\mathbf{G}_1$ is the gravity field vector. Displacement vector $\mathbf{X} = [\mathbf{u}_1 \ \mathbf{u}_2 \ ... \ \mathbf{u}_6]^T$, among them $\mathbf{u}_i = [x_i \ y_i \ \theta_{xi} \ \theta_{yi}]$, $i = 1, 2, ..., 24$, x_i, y_i and θ_{xi}, θ_{yi} are the vibration displacement and angular displacement of the i-th node on the x axes and y axes respectively.

System material damping considers the proportional damping (also known as Rayleigh damping) widely used in engineering. The following relationships exist.

$$\mathbf{C} = \alpha\mathbf{M} + \beta\mathbf{K}, \tag{10}$$

where $\alpha = 2(\xi_2/\omega_2 - \xi_1/\omega_1)/(1/\omega_2^2 - 1/\omega_1^2)$, $\beta = 2(\xi_2\omega_2 - \xi_1\omega_1)/(\omega_2^2 - \omega_1^2)$, ω_1 and ω_2 are the first two natural frequencies of the system, ξ_1 and ξ_2 are damping coefficients of the system.

Solving the dynamic equation of the outer race of rolling bearing with Newton's second law is as follows.

$$\begin{cases} m_{bi}\ddot{x}_{bi} + c_{bi}\dot{x}_{bi} + k_{bi}x_{bi} = F_{xri}, \\ m_{bi}\ddot{y}_{bi} + c_{bi}\dot{y}_{bi} + k_{bi}y_{bi} = F_{yri} - m_{bi}g, \end{cases} \tag{11}$$

where F_{xri} and F_{yri} ($i = 1, 2$) are the non-linear Hertz contact forces in the x and y directions on the outer rings of the left and right bearings respectively, they are opposite to the bearing support forces on both ends of the shaft.

Assuming that the outer ring of the bearing is firmly connected to the bearing seat, the inner ring rotates with the shaft. Let the displacement of the m-th node of the rotor be x_{rm} and y_{rm}, $x = x_{rm} - x_{bi}$, $y = y_{rm} - y_{bi}$. Substituting x and y into Eq. (11) obtains the bearing force acting on the i-th support by the rotor.

$$\begin{cases} F_{rxi} = K_b\sum_{j=1}^{N_b}(x\cos\theta_j + y\sin\theta_j - \delta_0)^{1.5}H(x\cos\theta_j + y\sin\theta_j - \delta_0)\cos\theta_j, \\ F_{ryi} = K_b\sum_{j=1}^{N_b}(x\cos\theta_j + y\sin\theta_j - \delta_0)^{1.5}H(x\cos\theta_j + y\sin\theta_j - \delta_0)\sin\theta_j. \end{cases} \tag{12}$$

Based on Eq. (9), considering the degree of freedom of the outer ring of the supporting bearing at both ends of the rotor system, the dynamic equation of the whole system can be obtained as follows.

$$\bar{M}\ddot{X} + (\bar{C} - \omega\bar{G} + \bar{C}_b)\dot{X} + (\bar{K} + \bar{K}_b)X = \bar{F}_e + \bar{F}_b + \bar{F}_h + \bar{G}_1, \tag{13}$$

where,

$$\bar{\mathbf{M}} = \begin{bmatrix} \mathbf{M} & & & & \\ & m_{b1} & & & \\ & & m_{b1} & & \\ & & & m_{b2} & \\ & & & & m_{b2} \end{bmatrix}, \quad \bar{\mathbf{C}} = \begin{bmatrix} \mathbf{C} & & & & \\ & c_{b1} & & & \\ & & c_{b1} & & \\ & & & c_{b2} & \\ & & & & c_{b2} \end{bmatrix},$$

$$\bar{\mathbf{G}} = \begin{bmatrix} \mathbf{G} & & & & \\ & 0 & & & \\ & & 0 & & \\ & & & 0 & \\ & & & & 0 \end{bmatrix}, \quad \bar{\mathbf{K}} = \begin{bmatrix} \mathbf{K} & & & & \\ & k_{b1} & & & \\ & & k_{b1} & & \\ & & & k_{b2} & \\ & & & & k_{b2} \end{bmatrix}, \quad \bar{U} = \begin{bmatrix} X & x_{b1} & y_{b1} & x_{b2} & y_{b2} \end{bmatrix}^{\mathrm{T}},$$

$$\mathbf{F}_e = \begin{bmatrix} 0,0,0,0,m_1e_1\omega^2\cos\omega t, m_1e_1\omega^2\sin\omega t, 0,0,0,0,0,0,0,0, \\ 0,0,m_2e_2\omega^2\cos\omega t, m_2e_2\omega^2\sin\omega t, 0,0,0,0,0,0,0,0,0,0 \end{bmatrix}^{\mathrm{T}},$$

$$\bar{\mathbf{G}} = [0,0,0,0,0,-m_1g,0,0,0,0,0,0,0,0,0,0,0,-m_2g,0,0,0,0,0,0,0,-m_{b1}g,0,-m_{b2}g]^{\mathrm{T}},$$

$$\bar{\mathbf{F}}_b = [-F_{bx1}, -F_{by1}, 0,0,0,0,0,0,0,0,0,0,0,0,0,0,0,0,0,0,-F_{bx2}, -F_{by2}, 0,0, F_{bx1}, F_{by1}, F_{bx2}, F_{by2}]^{\mathrm{T}},$$

where $\bar{\mathbf{F}}_h$ is the maneuver load vector.

This paper only discusses the influence of the maneuver load on the disc and bearing, regardless of the effect of the maneuver load on the shaft, so when the aircraft is in horizontal yawing motion, the maneuver load vector is [3].

Table 1. Simulation parameters of the rotor-bearing system

Parameters	Value
E (GPa)	209
v	0.3
ρ (kg/m^3)	7850
m_1, m_2 (kg)	15, 20
r (mm)	20
J_{d1}, J_{d2} (kg/m^2)	0.0375, 0.2
k_{b1}, k_{b2} (N/m)	2.5e6
c_{b1}, c_{b2} (N m/s)	1050
l_1, l_2, l_3, l_4, l_5 (m)	0.1, 0.2, 0.15, 0.05, 0.1
ξ_1, ξ_2	0.02, 0.04

Table 2. Natural frequencies of different models

Mode No.	ANSYS model		The present model	
	ω_n/Hz	ω_n/Hz	ω_n/Hz	ω_n/Hz
	(0 r/min)	(2000 r/min)	(0 r/min)	(2000 r/min)
Mode 1	96.384	94.88	96.03	94.22
	96.386	97.682	96.04	97.89
Mode 2	182.02	173.08	182.15	179.56
	182.04	190.2	182.15	184.78
Mode 3	294.49	277.64	295.36	291.20
	294.6	315.4	295.36	299.59

$$\overline{\mathbf{F}}_h = \begin{bmatrix} 0,0,0,0,m_1\omega_{B,y}v,0,J_{p1}\omega\omega_{B,y},0,0,0,0,0,0,0,0,0,0, \\ 0,0,0,m_2\omega_{B,y}v,0,J_{p2}\omega\omega_{B,y},0,m_{b1}\omega_{B,y}v,0,m_{b2}\omega_{B,y}v,0 \end{bmatrix}^{\mathrm{T}} \tag{14}$$

where $\omega_{B,y}$ is the yawing angular velocity, v is the navigation speed.

3. MODEL COMPARISON AND VERIFICATION

In order to test the validity of the model in this paper, in this section, the modal results obtained by the finite element calculation of ANSYS R2018 software and the modal results of the dynamic model built in this paper are compared and verified. In order to facilitate a better comparison between the modal results of the ANSYS model and the modal results of the model in this paper, the solid modeling of the bearing is ignored, and only the stiffness and damping in the x and y directions of the bearing are considered. The specific model and model parameters are shown in Fig. 3 and Table 1 below.

The natural frequency and mode shape of a rotor-bearing system are very important to the validity test of the model. The natural frequencies obtained based on the dynamic model method established in this paper and the natural frequencies obtained by the ANSYS model simulation are shown in Table 2. The Campbell diagram and the first three-order mode shapes are shown in Figs. 4 and 5 respectively. It can be seen from Table 2 and Fig. 4 that the first-order natural frequency of the present model is almost the same as that of the ANSYS model, and the relative error between the second and third-order natural frequencies is small, and the Campbell diagrams of the two models are basically similar. At the same time, it can be seen from Fig. 5 that the first three-order mode shapes of the two different models are also consistent.

Through the above comparison, it can be seen that the simulation results of the models built by the two different methods are basically the same, which fully verifies the effectiveness of the dynamic model
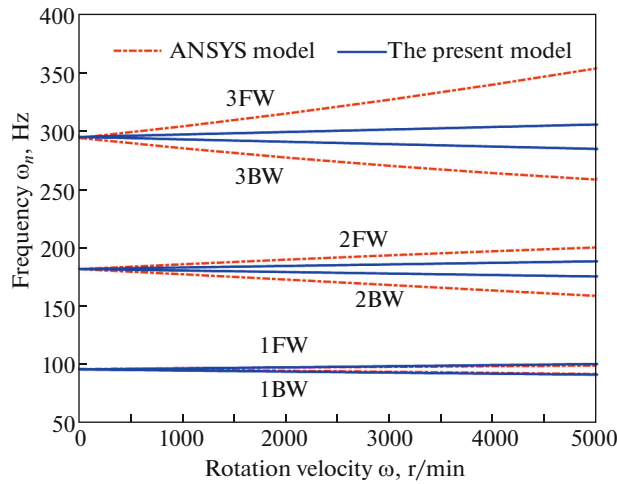
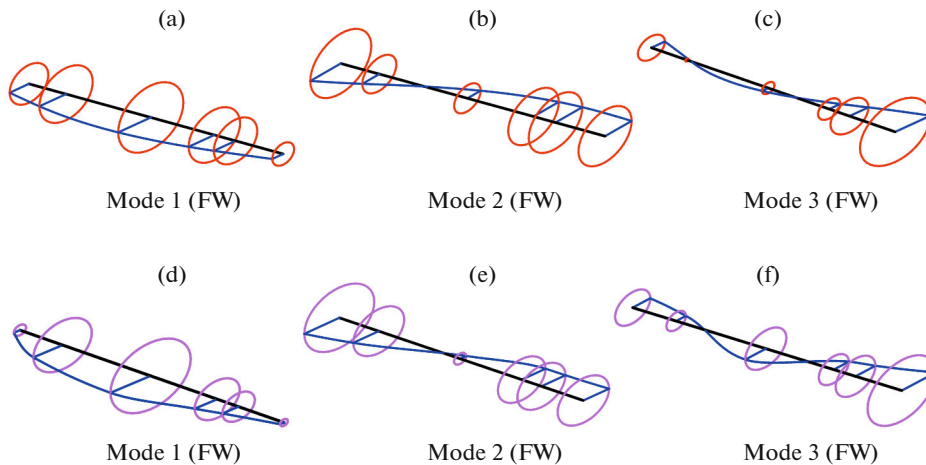**Fig. 4.** Campbell diagrams of two models. Note: FW indicates forward whirl and BW backward whirl.

Fig. 5. Mode shapes of two models at $\omega = 2000$ rad/s: (a)ANSYS model; (b) the present model.

method built in this paper. Therefore, in the next sections, we will use the dynamic model established in this paper to carry out numerical simulation.

4. NONLINEAR DYNAMICS ANALYSIS OF ROTOR-BEARING SYSTEM UNDER HORIZONTAL YAWING

In the study of nonlinear characteristics of rotor system, the vibration and bifurcation characteristics of the system are very worthy of attention. This section studies the vibration and bifurcation characteristics of the rotor system of an aircraft under the condition of maneuver flight in order to reveal the influence of maneuver loads on the nonlinear vibration and bifurcation characteristics of the rotor system. In essence, maneuver flight is a transient process, but compared with the vibration frequency of high-speed rotating rotor system, the change of maneuver load is very slow, which can be regarded as a slowly varying parameter. Due to the large complex nonlinear dynamic equation cannot give a clear analytical solution, this section uses MATLAB numerical simulation to analyze the nonlinear dynamic phenomenon of the system.

In order to more clearly express the main content of the latter part, Fig. 6 shows the detailed simulation process.

The simulation parameters of the rotor-bearing system are shown in Table 3.
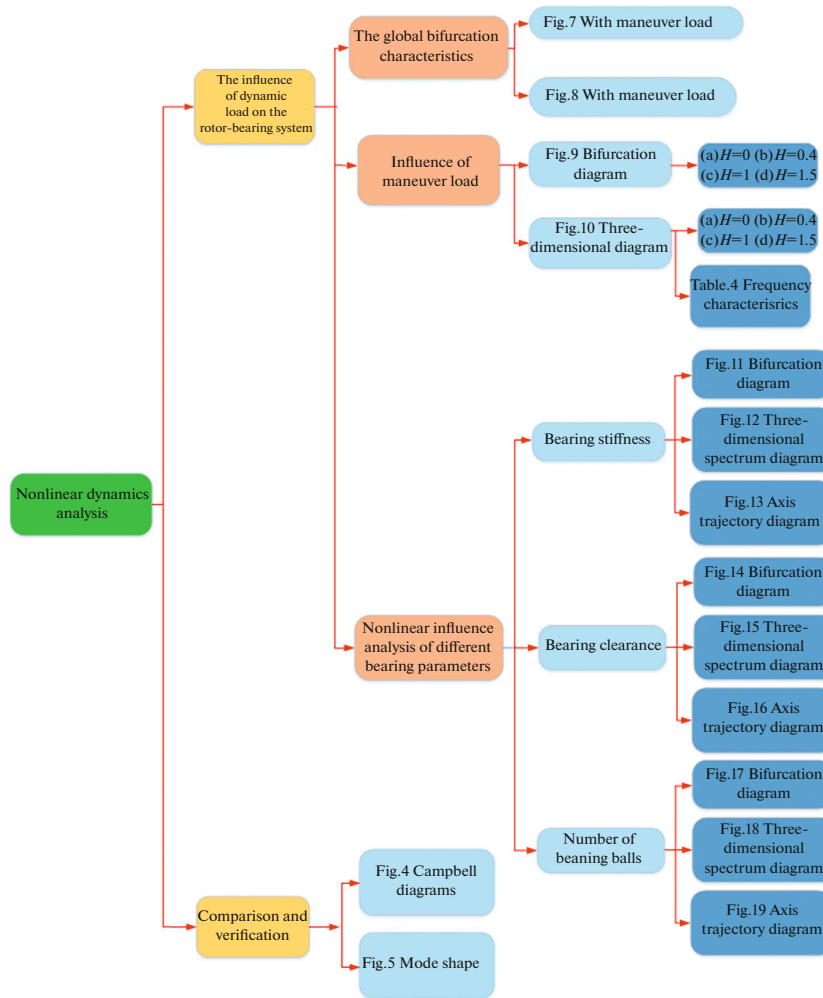
Fig. 6. The flow chart of simulation analysis.

4.1. Global Bifurcation Characteristics of The Rotor System With or Without Maneuver Load

In this paper, let $H = \omega_y V / g$ be the horizontal yawing maneuver load ($g = 10$ m/s^2). Figure 7 is the bifurcation diagram of the rotor-bearing system without maneuver load ($H = 0$). It can be seen the system moves in single-periodic when $\omega = 500{\sim}700$ rad/s. When the speed is around $\omega = 625$ rad/s, the system jumps to the maximum amplitude, it is known to be the first order critical speed ω_c. The system moves in single-period between $\omega = 700$ rad/s and $\omega = 1025$ rad/s, and perform multiple period bifurcation between $\omega = 1050$ rad/s and $\omega = 1150$ rad/s. When the system reaches two times the critical speed, that is the velocity is in the range of $\omega = 1225{\sim}1800$ rad/s, at this time, the main motion forms of the system are quasi-period and single-period, accompanied by multiple periods. When $\omega = 1450$ rad/s, the system moves in two-period. When $\omega = 1800$ rad/s, the system moves in triple period. When $\omega > 1800$ rad/s, the system moves in quasi-periodic.

Figure 8 shows the bifurcation diagram of the rotor-rolling bearing system with maneuver load (the maneuver load is $H = 0.4$). It can be seen the rotor-bearing system goes into single-periodic motion and multi-periodic motion alternately when $\omega < 1275$ rad/s. The motion interval of single-periodic motion of the rotor-bearing system are $\omega = 500$ rad/s$\sim$675 rad/s and $\omega = 825$ rad/s$\sim$1025 rad/s. The system goes into quasi-periodic motion and single-periodic motion successively between $\omega = 1300$ rad/s and $\omega = 1450$ rad/s. The rotor system goes into quasi-periodic motion when $\omega = 1450{\sim}1900$ rad/s, and the rotor-bearing system goes into quasi-periodic bifurcation when $\omega = 1850$ rad/s. The rotor system enters two-periodic motion after $\omega = 1925$ rad/s, and then goes approximate single-periodic motion when $\omega = 2000$ rad/s. The rotor system goes quasi-periodic motion when $\omega > 2250$ rad/s.

**Table 3.** Simulation parameters of the rotor-bearing system

Parameters	Value
E (GPa)	209
v	0.3
ρ (kg/m^3)	7850
m_1, m_2, m_{b1}, m_{b2}(kg)	15, 20, 2
e(mm)	0.02
r(mm)	20
J_{d1}, J_{d2} (kg m^2)	0.0375, 0.2
k_{b1}, k_{b2} (N/m)	2.5e7
c_{b1}, c_{b2} (N m/s)	1050
l_1, l_2, l_3, l_4, l_5(m)	0.1, 0.2, 0.15, 0.05,0.1
r_i, r_o(mm)	20.1, 43.9
δ_0(mm)	0.05
K_b(N/m)	5e9
N_b	9
ω_H(rad/s)	0.05
v (m/s)	100
g (m/s^2)	9.8

Compared with the rotor-bearing-rotor system without maneuver load, the rotor-bearing system with maneuver load is relatively stable at high speed and has small amplitude. This is a consequence of the fact that the sum of the maneuver load excitation and the unbalanced excitation is greater than the nonlinear force of the rolling bearing at high speed.

4.2. The Influence of Maneuver Load on the Bifurcation Characteristics of the Rotor System

When the maneuver loads are $H = 0$, $H = 0.4$, $H = 1$ and $H = 1.5$, the bifurcation diagrams of the rotor-bearing system at general engine speed (1000 rad/s~2000 rad/s) are shown in Figs. 9a, 9b, 9c and 9d. Compared with the without maneuver load in Fig. 9a, the system with maneuver load has a large nonlinear dynamic change, it can be seen the maneuver load has a very significant effect on the nonlinear vibration characteristics of the rotor system. With the increase of H, the amplitude of the rotor-bearing system is
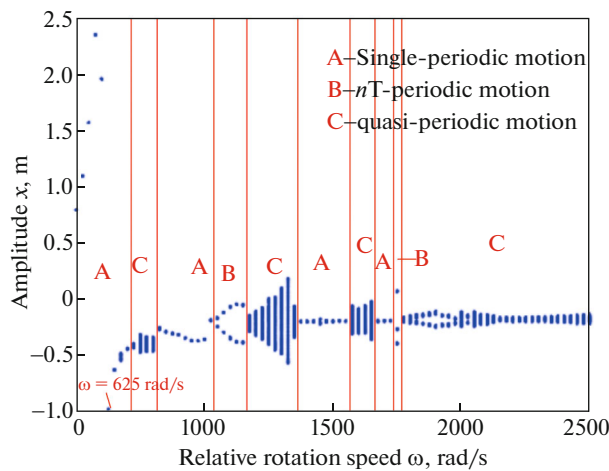
Fig. 7. Bifurcation diagram without maneuver load.
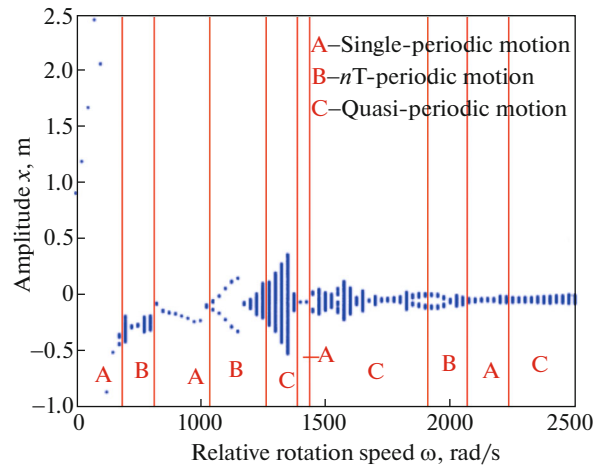
Fig. 8. Bifurcation diagram with maneuver load.

getting smaller and more stable, the quasi-periodic bifurcation point of the rotor-bearing system moves back. The proportion of quasi-periodic motion between $\omega = 1000$ rad/s and $\omega = 2000$ rad/s decreases, the proportion of single-periodic motion and multi-periodic motion increased. It is known that the critical speed of the primary resonance increases, it can be seen the existence of maneuver load is equivalent to increasing the stiffness of the shaft. But with the increase of maneuver load H, the stability of the system has improved, the proportion of quasi-periodic motion decreases gradually, the proportion of single-periodic motion gradually increases. For example, when there is no maneuver load, the system mainly moves in quasi-period. When the maneuver load H reaches 1.5, the system is mainly single-periodic motion. This is because the maneuver load excitation is greater than the non-linear force of the rolling bearing, which suppresses the nonlinear vibration of the system.

In order to analyze the complex nonlinear phenomenon in bifurcation diagram, the spectrum cascade as shown in Fig. 10 is given. It can be seen from the figure that the whole system is mainly low-frequency vibration, and there are low-frequency components such as $0.33f_r$, $0.48f_r$, $0.5f_r$, and $0.56f_r$ when $H = 0$. When the system speed reaches twice the first-order critical speed ($\omega = 2\omega_c$), the first-order vibration frequency component of the rotor appears in the system, which indicates that 1/2 subharmonic vibration occurs in the system at this moment. Subharmonic vibration is very common in the rotor-bearing system. And with the increase of maneuver load H, the low frequency component of the system frequency decreases gradually, the overall system frequency will increase, and the system nonlinearity will decrease. Therefore, it is concluded that the reduction of the system non-linear vibration is due to the increase of the maneuver load.

4.3. Nonlinear Influence of Different Bearing Parameters on the System

4.3.1. Nonlinear Influence of Bearing Stiffness on the System

This section analyzes the vibration response of different bearing stiffness changes with or without maneuver load. Figures 11 and 12 respectively show the bifurcation diagram and three-dimensional spectrum diagram of bearing stiffness changes with or without maneuver load. It can be seen from Fig. 11a that the single periodic region is ([0.1e9,0.5e9]; [1.8e9,2.6e9]; [3e9,4.3e9]), and the double periodic region is ([1e9,1.1e9]; [2.7e9,2.9e9]), and the quasi periodic region is ([0.6e9,0.9e9]; [1.09,1.7e9]; [4.4e9,8e9]). It can be seen from Fig. 11b that the single periodic region is ([0.1e9,0.4e9]; [1.6e9,4e9]), and the double periodic region is ([0.5e9,1.5e9]), and the quasi periodic region is ([4.1e9,8e9]). As can be seen from Fig. 12, there are more frequency division components in the system when there is no maneuver load, and the movement is more chaotic. Through comparative analysis, it can be seen that when the system has a maneuver load value, the single periodic region increases, the quasi periodic region decreases, the frequency division decreases, and the vibration displacement of the system decreases with the increase of bearing stiffness in the single periodic region. This indicates that maneuver load can reduce the nonlinear influence of bearing stiffness change on the system, so that bearing stiffness has a wider range of values, and the nonlinear behavior of the system gradually becomes complex with the increase of bearing stiffness. when the bearing stiffness is large, the system shows chaotic motion, that is, the greater the bearing stiffness, the more complex the vibration response of the system. The specific periodic changes are shown in Table 5.
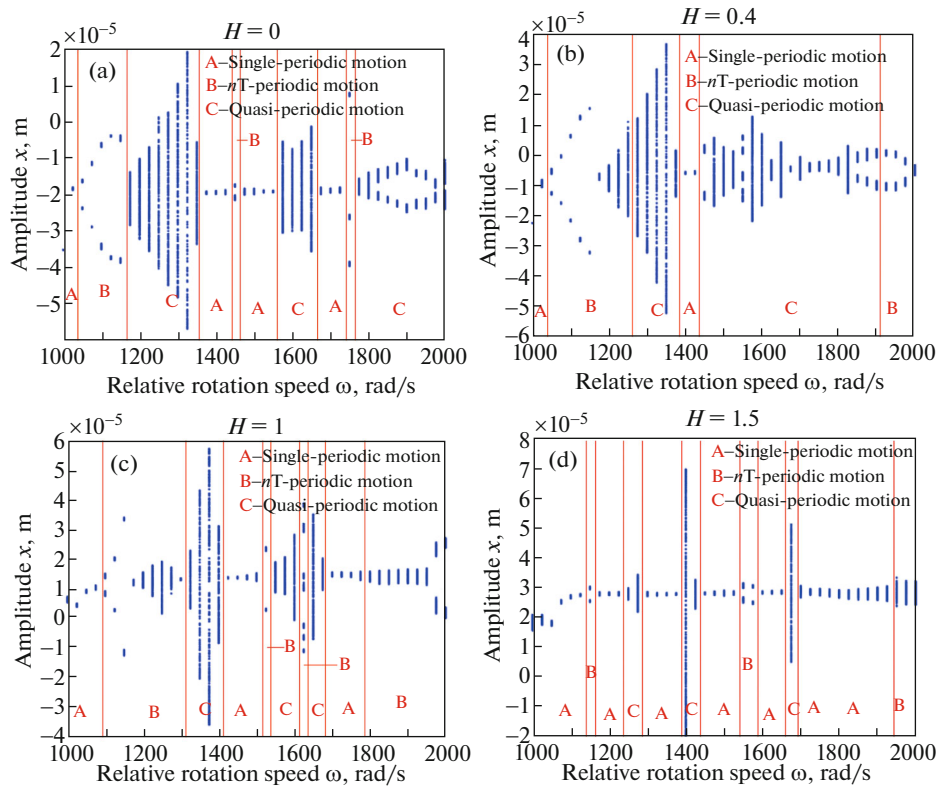
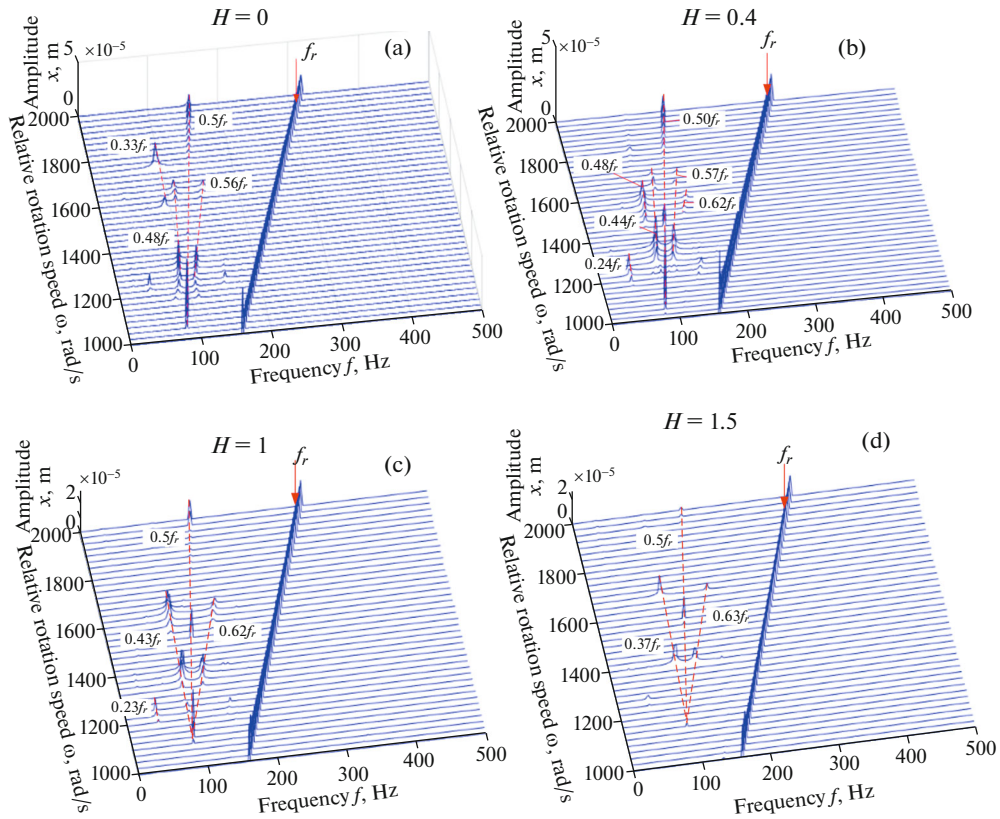**Fig. 9.** Bifurcation diagram of the rotor system under different maneuver loads.

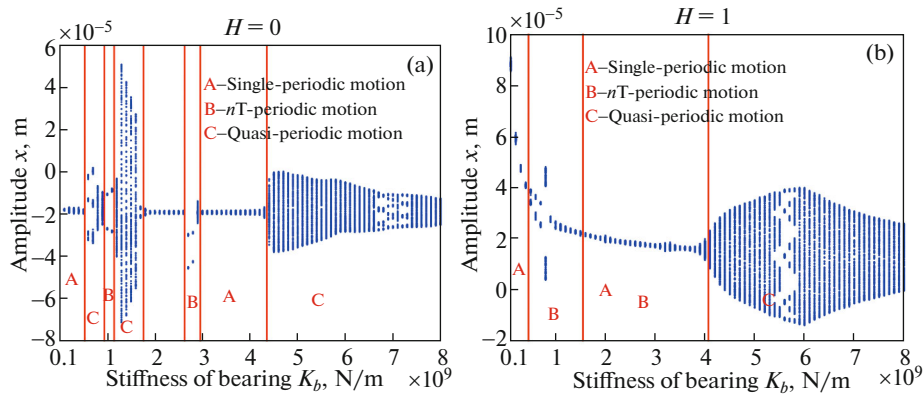**Fig. 10.** Three-dimensional spectrogram of rotor system under different maneuver loads.

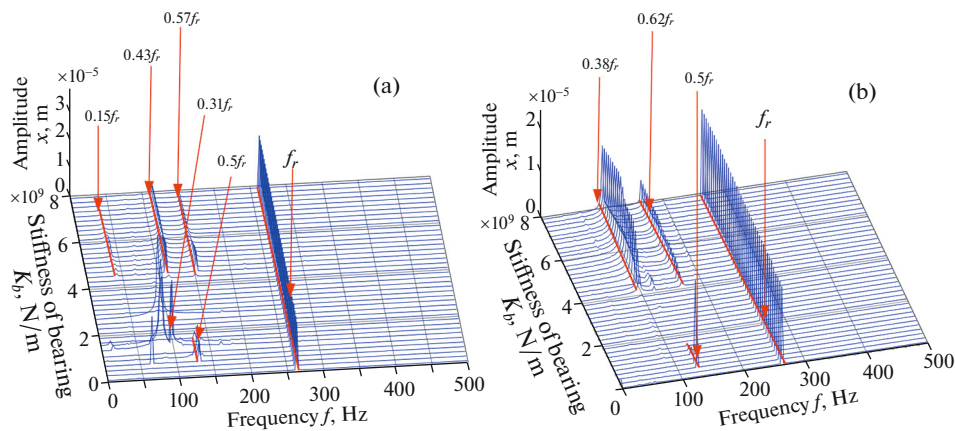**Fig. 11.** Bifurcation diagram of bearing stiffness change with or without maneuver load.

Fig. 12. Three-dimensional spectrum diagram of bearing stiffness change with or without maneuver load.

In order to better analyze the dynamic response law of bearing stiffness change with or without maneuver load, Fig. 13 shows the axis trajectory diagram with or without maneuvering load. As can be seen from Fig. 13, the vibration displacement in the x direction of the system with maneuver load is smaller than that without maneuver load, and the movement period is approximately elliptical, and the movement behavior of the system becomes more complex with the increase of bearing stiffness. This fully shows that the maneuver load can reduce the dynamic response of bearing stiffness changes to the system, and that larger bearing stiffness will make the motion behavior of the system more complex.

4.3.2. Nonlinear Influence of Bearing Clearance on the System

This section analyzes the vibration response of different bearing clearance changes with or without maneuver load. Fig. 14 and Fig. 15 respectively show the bifurcation diagram and three-dimensional spectrum diagram of bearing clearance changes with or without maneuver load. It can be seen from Fig. 14a that the single periodic region is ([0,0.3e-5]; [0.21e-5,0.36e-5]), and the double periodic region is ([0.06e-5,0.18e-5]), and the quasi periodic region is ([0.39e-5,2e-5]). It can be seen from Fig. 14b that the single periodic region is ([0,1.17e-5]), and no double periodic region, and the quasi periodic region is ([1.5e-5,2e-5]). It can be seen from Fig. 15 that there are more frequency components when there is no maneuver load than when there is maneuver load, and the motion behavior of the system is more chaotic, and with the increase of bearing clearance, the vibration response of the system becomes more complex. Through the comparative analysis of bearing clearance changes with or without maneuver load, it can be seen that the maneuver load increases the single periodic region and decreases the quasi periodic region, effectively reducing the bifurcation type of the system, so that the bearing clearance has a wider range of values. It is shown that maneuver load can reduce the system nonlinear response caused by bearing clearance change. The specific periodic changes are shown in Table 6.

Table 4. Frequency characteristics under different maneuver loads

Maneuver loads	Relative rotation speeds(rad/s)	Frequency characteristics
$H = 0$	$1000 \leq \omega < 1050$	f_r
	$1050 \leq \omega < 1250$	$0.5f_r, f_r$
	$1250 \leq \omega < 1350$	$0.48\,f_r, 0.5f_r, 0.56\,f_r, f_r$
	$1350 \leq \omega < 1575$	f_r
	$1575 \leq \omega < 1600$	$0.33\,f_r, f_r$
	$1600 \leq \omega < 1650$	$0.48\,f_r, 0.56f_r, f_r$
	$1650 \leq \omega < 1750$	f_r
	$1750 \leq \omega < 1775$	$0.33\,f_r, f_r$
	$1775 \leq \omega \leq 2000$	$0.5f_r, f_r$
$H = 0.4$	$1000 \leq \omega < 1050$	f_r
	$1050 \leq \omega < 1200$	$0.5f_r, f_r$
	$1200 \leq \omega < 1275$	$0.24f_r, 0.5f_r, f_r$
	$1275 \leq \omega \leq 1350$	$0.44f_r, 0.5f_r, 0.57f_r, f_r$
	$1350 < \omega < 1450$	f_r
	$1450 \leq \omega \leq 1475$	$0.48f_r, 0.5f_r, f_r$
	$1475 < \omega \leq 1600$	$0.44f_r, 0.62f_r, f_r$
	$1600 < \omega < 1725$	$0.44f_r, 0.57f_r, f_r$
	$1725 \leq \omega \leq 2000$	$0.5f_r, f_r$
$H = 1$	$1000 \leq \omega < 1100$	f_r
	$1100 \leq \omega < 1200$	$0.5f_r, f_r$
	$1200 \leq \omega \leq 1250$	$0.23f_r, 0.43f_r, f_r$
	$1250 < \omega < 1325$	f_r
	$1325 \leq \omega < 1425$	$0.43f_r, 0.62f_r, f_r$
	$1425 \leq \omega < 1525$	f_r
	$1525 \leq \omega < 1550$	$0.5f_r, f_r$
	$1550 \leq \omega < 1675$	$0.43f_r, 0.62f_r, f_r$
	$1675 \leq \omega < 1800$	f_r
	$1800 \leq \omega \leq 2000$	$0.5f_r, f_r$
$H = 1.5$	$1000 \leq \omega < 1150$	f_r
	$1150 \leq \omega < 1200$	$0.5f_r, f_r$
	$1200 \leq \omega < 1400$	f_r
	$1400 \leq \omega < 1450$	$0.37f_r, 0.63f_r, f_r$
	$1450 \leq \omega < 1550$	f_r
	$1550 \leq \omega < 1600$	$0.5f_r, f_r$
	$1600 \leq \omega < 1675$	f_r
	$1675 \leq \omega < 1700$	$0.37f_r, 0.63f_r, f_r$
	$1700 \leq \omega < 1950$	f_r
	$1950 \leq \omega < 2000$	$0.5f_r, f_r$

Table 5. Comparison of periodic region of bearing stiffness change with or without maneuver load

| Maneuver load	Single periodic region	Double periodic region	Quasi periodic region
$H = 0$	[0.1e9,0.5e9]; [1.8e9,2.6e9]; [3e9,4.3e9]	[1e9,1.1e9]; [2.7e9,2.9e9]	[0.6e9,0.9e9]; [1.e9,1.7e9] [4.4e9,8e9]
$H = 1$	[0.1e9,0.4e9]; [1.6e9,4e9]	[0.5e9,1.5e9]	[4.1e9,8e9]

Table 6. Comparison of periodic region of bearing clearance change with or without maneuver load

Maneuver load	Single periodic region	Double periodic region	Quasi periodic region
$H = 0$	[0,0.3e-5]; [0.21e-5,0.36e-5]	[0.06e-5,0.18e-5]	[0.39e-5,2e-5]
$H = 2$	[0,1.17e-5]	None	[1.5e-5,2e-5]

In order to better analyze the dynamic response law of bearing clearance change with or without maneuver load, Fig. 16 shows the axis trajectory diagram with or without maneuvering load. As can be seen from Fig. 16, the axial trajectory range of the system with a maneuver load is always smaller than the axial trajectory range without maneuver load, and the movement period of the system changes from single periodic to quasi periodic with the increase of bearing clearance. This shows that the better the vibration response of the system under maneuver load, the dynamic load can reduce the nonlinear response of the system caused by the change of bearing clearance.

4.3.3. Nonlinear Influence of the Number of Bearing Balls on the System

This section analyzes the vibration response of different bearing ball numbers changes with or without maneuver load. Figs. 17 and 18 respectively show the bifurcation diagram and three-dimensional spectrum diagram of different bearing ball numbers changes with or without maneuver load. It can be seen
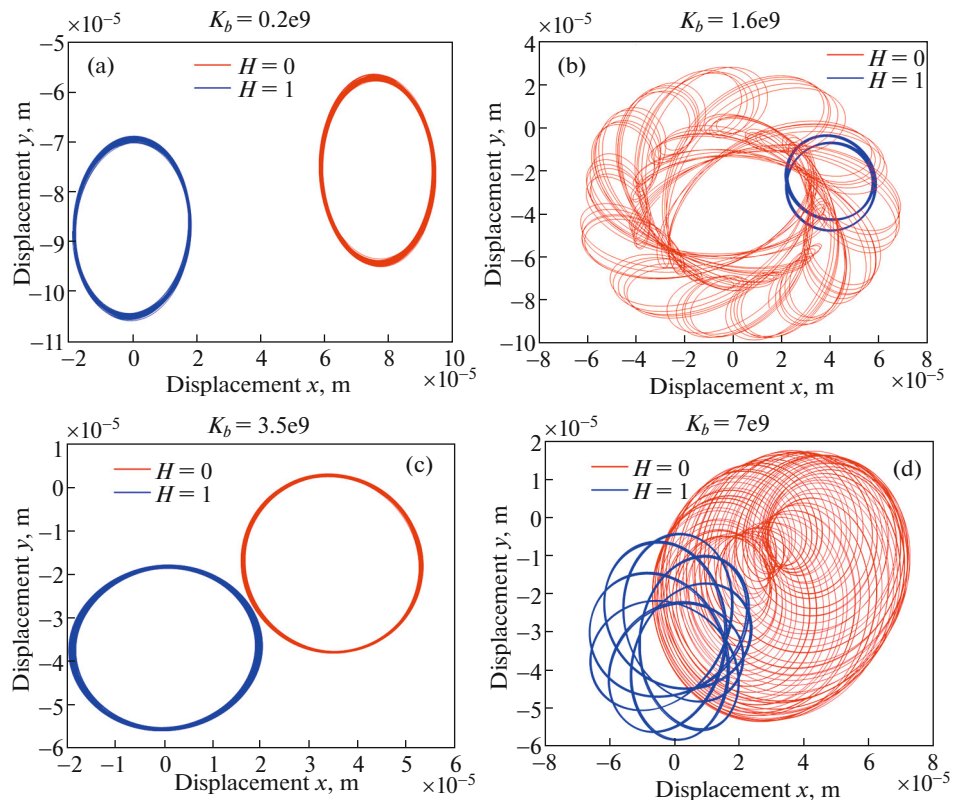
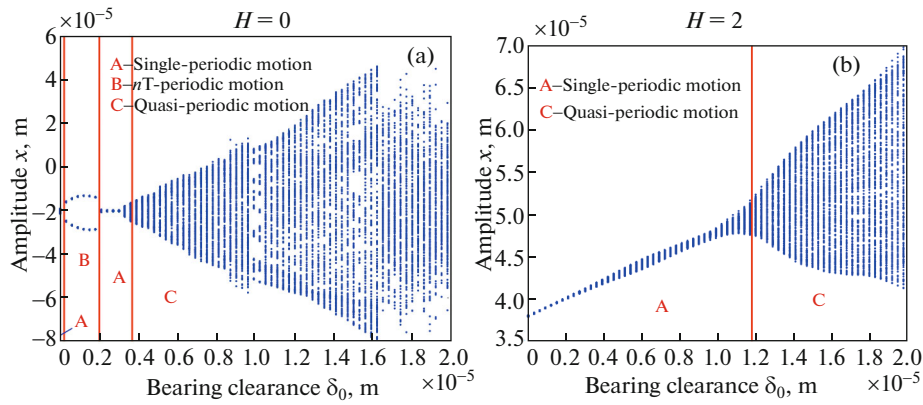**Fig. 13.** Axis trajectory diagram of bearing stiffness change with or without maneuver load.

Fig. 14. Bifurcation diagram of bearing clearance change with or without maneuver load.
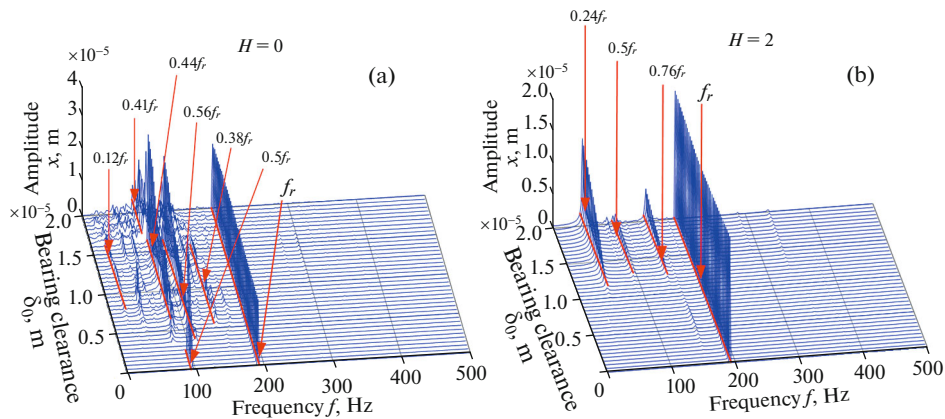

Fig. 15. Three-dimensional spectrum diagram of bearing clearance change with or without maneuver load.

from Fig. 17a that the single periodic region is ([5]; [13,30]), and no double periodic region, and the quasi periodic region is ([4], [6, 12]). It can be seen from Fig. 17b that the single periodic region is ([7, 10], [15, 30]), and double periodic region is ([10, 14]), and the quasi periodic region is ([4, 5]). It can be seen from Fig. 18 that when the number of balls is small, the system has more frequency division components. Through the bifurcation diagram and three-dimensional spectrum diagram with or without maneuver load, it can be clearly seen that the system behaves as a single periodic motion when the number of balls is taken at a larger value, and the system behaves as a quasi-periodic motion when the number of balls is taken at a smaller value, and the maneuver load increases the single periodic region, that is, the maneuver load reduces the nonlinear vibration response of the system caused by the change of the number of balls. The specific periodic changes are shown in Table 7.

In order to better analyze the dynamic response law of different bearing ball numbers change with or without maneuver load, Fig. 19 shows the axis trajectory diagram with or without maneuvering load. As can be seen from Fig. 19, the maneuver load makes the axis motion trajectory more regular, and the vibration displacement in the y direction of the system is smaller than the vibration displacement in the y direction without the maneuver load, and the axis trajectory is approximately circular when the number of balls is larger. Therefore, the maneuver load and the large number of balls can reduce the nonlinear response of the system caused by the change of the number of bearing balls.

5. CONCLUSIONS

In this paper, the non-linear dynamic characteristics of an aero-engine rotor system under horizontal maneuver flight are studied in detail. The main research results of this paper are as follows.
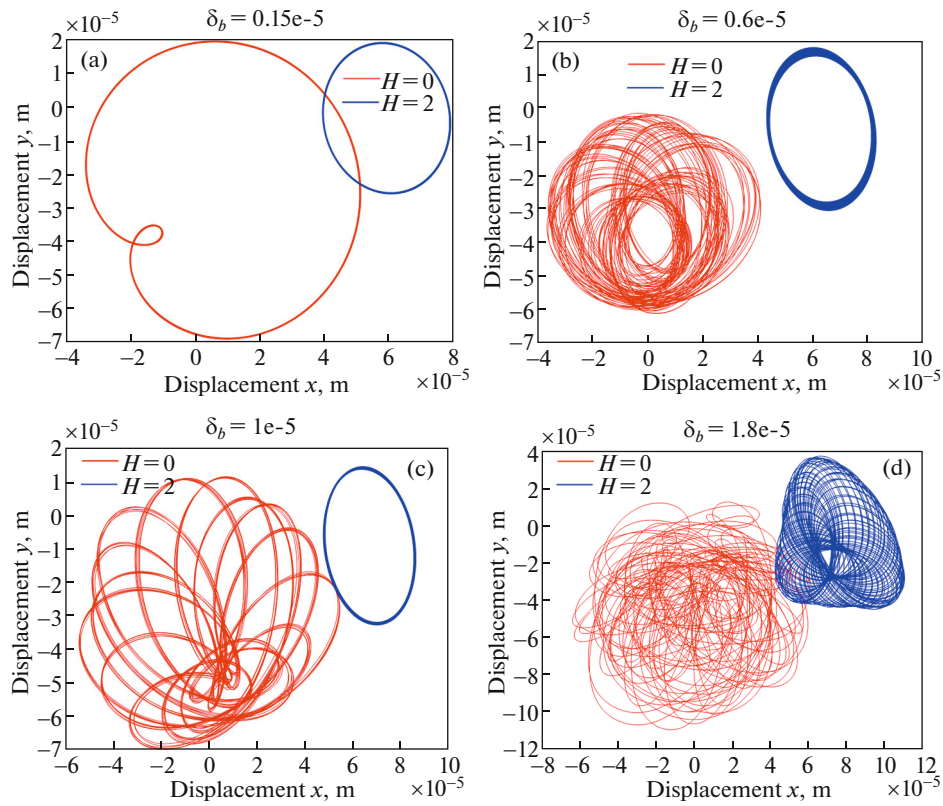
Fig. 16. Axis trajectory diagram of bearing clearance change with or without maneuver load.
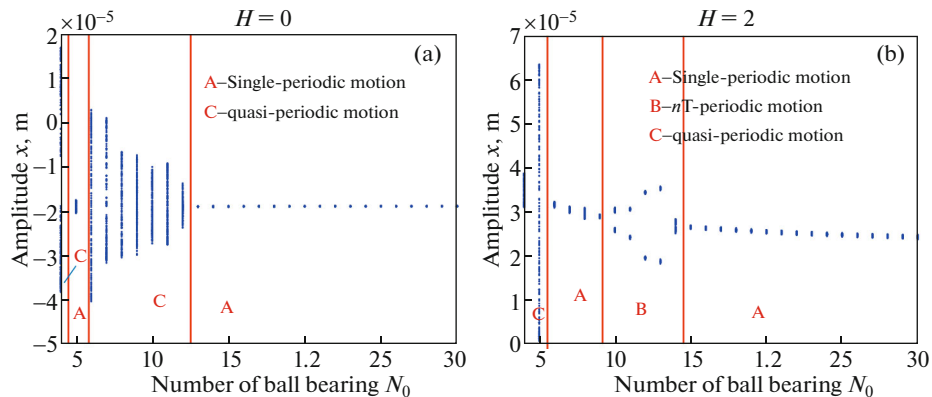

Fig. 17. Bifurcation diagram of different bearing ball numbers change with or without maneuver load.

(1) Under the condition of the horizontal yawing maneuver flight, when the rotation speed of the rotor system is between one critical speed and two times critical speed, the system movement is relatively simple, with only single-periodic motion and multi-periodic motion; when the speed of the rotor system is

Table 7. Comparison of periodic region of different bearing ball numbers change with or without maneuver load

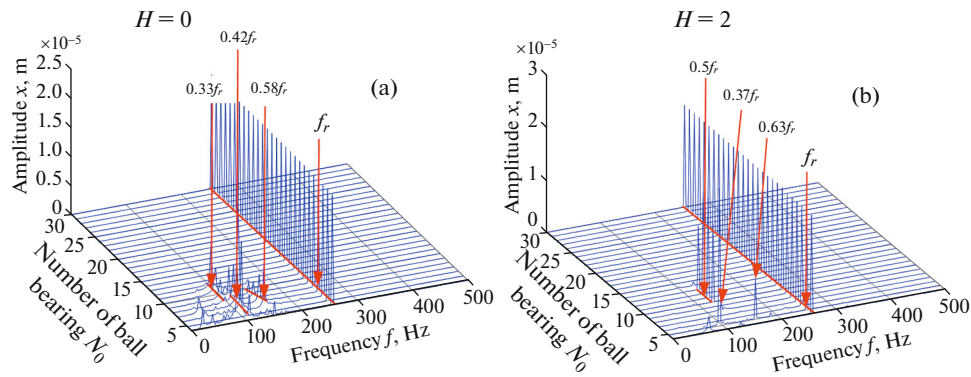| Maneuver load	Single periodic region	Double periodic region	Quasi periodic region
$H = 0$	[5]; [13,30]	None	[4], [6, 12]
$H = 1.5$	[7, 10], [15, 30]	[10, 14]	[4, 5]

Fig. 18. Three-dimensional spectrum diagram of different bearing ball numbers change with or without maneuver load.
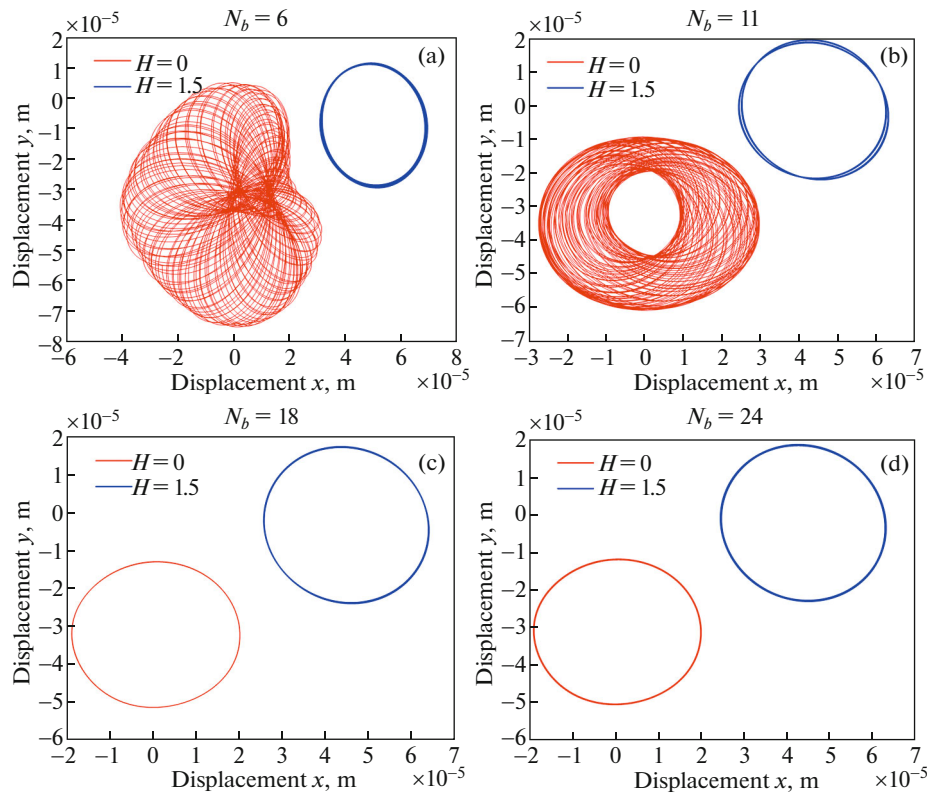

Fig. 19. Axis trajectory diagram of different bearing ball numbers change with or without maneuver load.

between two times critical speed and three times critical speed, the system will produce rich and complex nonlinear dynamic phenomena, such as single-periodic motion, multi-periodic motion and quasi-periodic motion.

(2) With the increase of the maneuver load H, the low frequency component of the system frequency decreases gradually, the overall system frequency increases, the nonlinear vibration of the system is weakened, due to the increase of the maneuver load.

(3) The larger the bearing stiffness and bearing clearance will enhance the nonlinear vibration response of the system, the larger the number of bearing balls will weaken the nonlinear vibration response of the system, and the increase of maneuver load can reduce the nonlinear influence of the system caused by changes in relevant bearing parameters.

Appendix

Nomenclature	
v_0, v_i (m/s)	Linear velocity of outer and inner ring contact points
ω_0, ω_i (rad/s)	Rotational angular velocity of outer and inner rings
R_0, R_i (mm)	Radius of outer and inner raceway
v_c (m/s)	Linear velocity of rolling body center
ω_c (rad/s)	First order critical speed
N_b	Number of bearing balls
δ_0 (mm)	Bearing radial clearance
k_b (N/m)	Hertz contact stiffness
F_{in}, F_{it} (N)	Normal and tangential rubbing force
μ_r (Pa · s)	Friction factor
m_1, m_2, m_{b1}, m_{b2} (kg)	Disc 1, 2, left and right end bearing ring mass
J_{di}, J_{pi} (kg/m^2)	Diameter, polar moment of inertia
k_{b1}, k_{b2} (N/m)	Stiffness of left and right outer ring connection
c_{b1}, c_{b2} (N m/s)	Connection damping of left and right outer rings
$\mathbf{F}_{xri}$, $\mathbf{F}_{yri}$ (N)	Nonlinear Hertz contact force of left and right rings
$\mathbf{C}_b$, $\mathbf{K}_b$	Damping matrix and stiffness matrix
$\mathbf{F}_h$	Nonlinear Hertz contact vector of rolling bearing
$\mathbf{F}_n$	Maneuver load vector
E (GPa)	Modulus of elasticity
v	Poisson's ratio
ρ (kg/m^3)	Material density
ω_y (rad/s)	Angular velocity around the y axis
V (m/s)	The forward speed of navigation

REFERENCES

1. J. Gao, P. S. Zhu, and Z. H. Gao, *Advanced Flight Dynamics* (National Defense Industry Press, Beijing, 2004).

2. W. B. Herbst, "Future fighter technologies," AIAA. J. **17** (8), 561−566 (1980).

3. C. S. Zhu and Y. J. Chen, "Unified model of engine rotor system dynamics during maneuvering flight," J. Aero. Dyn. **24**, 371−377 (2009).

4. W. J. Pan, L. Y. Ling, H. Y. Qu, and M. H. Wang, "Early wear fault dynamics analysis method of gear coupled rotor system based on dynamic fractal backlash," J. Comput. Nonlin. Dyn. **17** (1), 011003 (2022).
https://doi.org/10.1115/1.4052650

5. W. J. Pan, X. P. Li, L. L. Wang, and Z. M. Yang, "Nonlinear response analysis of gear-shaft-bearing system considering tooth contact temperature and random excitations," Appl. Math. Model. **68** (3), 113−136 (2019).
https://doi.org/10.1016/j.apm.2018.10.022

6. L. Ya. Banakh and A. N. Nikiforov, "Action of aerohydrodynamic forces on high-speed rotor systems," Mech. Solids **41** (5), 34−42 (2006).

7. Y. Xu and A. Luo, "Period-1 to period-8 motions in a nonlinear Jeffcott rotor system," J. Comput. Nonlin. Dyn. **15** (9), 091012 (2020).
https://doi.org/10.1115/1.4046714

8. P. P. Ma, J. Y. Zhai, and Z. H. M. Wang, "Unbalance vibration characteristics and sensitivity analysis of the dual-rotor system in aeroengines," J. Aerosp. Eng. **34** (1), 04020094 (2021).
https://doi.org/10.1061/(ASCE)AS.1943-5525.0001197

9. P. P. Ma, J. Y. Zhai, and H. Zhang, "Multi-body dynamic simulation and vibration transmission characteristics of dual-rotor system for aeroengine with rubbing coupling faults," J. Vibroeng. **21** (7), 1875−1887 (2019).
https://doi.org/10.21595/jve.2019.20206

10. W. Fan, J. L. Li, J. X. Liu, et al., "Aeroengine rotor system vibration characteristics under action of rotating stall transverse load," J. Aerosp. Pwr. **32** (5), 1120−1130 (2017).
https://doi.org/10.13224/j.cnki.jasp.2017.05.013

11. W. Fan, Master's Thesis (Huazhong Univ. Science & Tech., Huazhong, 2016).

12. H. P. Phadatare and B. Pratiher, "Nonlinear modeling, dynamics, and chaos in a large deflection model of a rotor−disk−bearing system under geometric eccentricity and mass unbalance," Acta. Mech. **231** (3), 907−928 (2020).
https://doi.org/10.1007/s00707-019-02559-9

13. H. R. Cao, Y. M. Li, and X. F. Chen, "A new dynamic model of ball-bearing rotor systems based on rigid body element," J. Manuf. Sci. Eng. **138** (7), 071007 (2016).
https://doi.org/10.1115/1.4032582

14. H. R. Cao, L. K. Niu, S. T. Xi, and X. F. Chen, "Mechanical model development of rolling bearing-rotor systems: A review." Mech. Syst. Signal. Pr. **102**, 37−58 (2018).
https://doi.org/10.1016/j.ymssp.2017.09.023

15. C. Fu, Y. D. Xu, Y. F. Yang, and K. Lu, "Dynamics analysis of a hollow-shaft rotor system with an open crack under model uncertainties," Commun. Nonlin. Sci. **83**, 1−18 (2020).
https://doi.org/10.1016/j.cnsns.2019.105102

16. S. P. Harsha and P. K. Kankar, "Stability analysis of a rotor bearing system due to surface waviness and number of balls," Int. J. Mech. Sci. **45** (7), 1057−1081 (2004).
https://doi.org/10.1016/j.ijmecsci.2004.07.007

17. S. P. Harsha, K. Sandeep, and R. Prakash, "Non-linear dynamic behaviors of rolling element bearings due to surface waviness," J. Sound Vib. **272** (3), 557−580 (2004).
https://doi.org/10.1016/S0022-460X(03)00384-5

18. M. Xu, M. F. Liao, and Q. Z. Liu, "The vibration performance of the double-disk cantilever rotor in flight mission," J. Aerosp. Pwr. **17** (1), 105−109 (2002).

19. M. Xu and M. F. Liao, "The vibration performance of the Jeffcott rotor system with SFD in maneuver flight," J. Aerosp. Pwr. **18** (3), 394−401 (2003).

20. F. S. Lin and G. Meng, "Research on the dynamic characteristics of the engine rotor and other variable-speed motions during the maneuvering flight." Acta. Aeronaut. Astron. Sin. **23** (4), 356−359 (2002).

21. C. S. Zhu, and Y. J. Chen, "Vibration characteristics of aeroengine's rotor system during maneuvering flight," Acta. Aeronaut. Astron. Sin. **27** (5), 835−841 (2006).

22. P. Gao and L. Hou, "Local defect modelling and nonlinear dynamic analysis for the inter-shaft bearing in a dual-rotor system," Appl. Math. Model. **68**, 29−47 (2019).
https://doi.org/10.1016/j.apm.2018.11.014

23. L. Hou, Y. S. Chen, and Q. J. Cao, "Turing maneuver caused response in an aircraft rotor-ball bearing system," Nonlin. Dyn. **79** (1), 229−240 (2015).
https://doi.org/10.1007/s11071-014-1659-8

24. Z. Lu, Y. Hou, L. Hou, and Y. Chen, "Dynamic characteristics of an aero-engine rotor system with crack faults," J. Vib. Shock. **37** (3), 40−46 (2018).
https://doi.org/10.13465/j.cnki.jvs.2018.03.007

25. P. Zhang, PhD Dissertation (Nanjing University Aeronautics and Astronautics, Nanjing, 2018).

26. T. Gao, S. Cao, and Y. Sun, "Nonlinear dynamic behavior of a flexible asymmetric aero-engine rotor system in maneuvering flight," Chin. J. Aeronaut. **10**, 2633−2648 (2020).
https://doi.org/10.1016/j.cja.2020.04.001

27. Z. X. Fei, "Research on finite element modeling and dynamic behaviors of complex multi-rotor coupled systems," Doctoral Dissertation (Zhejiang University, Zhejiang, 2013).

28. H. Ma, H. Li, X. Y. Zhao, et al., "Effects of eccentric phase difference between two discs on oil-film instability in a rotor−bearing system," Mech. Syst. Signal Proc. **41** (1−2), 526−545 (2013).
https://doi.org/10.1016/j.ymssp.2013.05.006

29. H. Ma, H. Li, H. Q. Niu, et al., "Nonlinear dynamic analysis of a rotor-bearing-seal system under two loading conditions," J. Sound. Vib. **332** (23), 6128−6154 (2013).
https://doi.org/10.1016/j.jsv.2013.05.014